The Structure and Variability of Active Galactic Nuclei

9-Month Report

S. D. Connolly

Supervisor: I.M. McHardy

ABSTRACT

Active galactic nuclei (AGN) are thought to be supermassive black holes at the centre of galaxies which are accreting nearby material. The nature of these black holes, their surroundings and their similarity to galactic black holes (GBHs), are currently a topic of great interest to researchers. By studying the spectra and variability of emission from such objects, we can learn a great deal about these subjects. In this work we present long-term X-ray spectral variability of the Seyfert galaxy NGC 1365. We find that the absorbing column decreases with increasing luminosity, but that this result is not due to changes in ionisation. We suggest that these observations might be interpreted in terms of a wind model in which the launch radius moves outwards with increasing luminosity. Thus, depending on the inclination angle of the disc relative to the observer, the absorbing column may decrease as the luminosity increases.

Further to this, we present a cross-correlation study of the nucleus of NGC 5548, a Seyfert galaxy, thought to be analogous to the 'high-soft' state of GBHs. The nucleus' lightcurves in radio, from *AMI*, and in X-rays, from *XMM Newton* and *SWIFT*, are found to be correlated with time lag of approximately 40 days between variations in the X-ray and the radio. It therefore follows that the nuclear radio emission is linked to the same process producing the X-ray emission.

CONTENTS

1 Introduction

Active Galactic Nuclei (AGN) are the central regions of 'active galaxies', thought to contain a supermassive black hole, which are of comparable or greater brightness than the galaxy itself (Krolik 1999). The structure of the surroundings of these black holes is a well studied but still largely unknown topic; the most popular theory invokes a unification of the many of types of AGN through geometry, involving a large accretion disc surrounded by a parsec-scale torus of dusty matter, a broad-line emission region between the two and an outer narrow-line region (Krolik & Bianchi (1988),Bianchi et al. (2012),Urry & Padovani (1995)). More recently, high-velocity features in AGN spectra have been attributed to an additional component, namely a 'wind' emanating from the accretion disc, possessing its own emission and absorption properties (Elvis 2000). The exact nature of these components and the accuracy of this model is, however, still unclear.

In addition to AGN structure, much recent research has looked into the possibility that the physics of black holes of all masses is the same, meaning the more detailed physics known about galactic black holes (GBHs) can be scaled up and applied to AGN (McHardy et al. 2006). GBHs are often classified as being in one of a number of 'states', believed to be dependent on the accretion rate in the system at the time of observation (McClintock & Remillard (2006), Fender et al. (2004)). The majority of a black hole's time is spent in either the 'low-hard state' or the 'high-soft state', defined according to its luminosity and the hardness of its X-ray spectrum (Jones et al. (2011), Belloni (2010)). It is also thought that radio-emitting jets are present only when in the low-hard state. Seyfert galaxies are considered to be candidates for 'high-soft' state AGN (McHardy et al. 2004). If this is the case, radio-emitting jets would not be expected in Seyfert galaxies. Radio variability has, however been detected in Seyfert galaxies, although not extensively (Neff & Bruyn (1983), Mundell et al. (2009)). In order to ascertain whether this radio emission is due to existing radio jets, a correlation needs to be found between this and emission in another waveband, e.g. X-rays. King et al. (2013) recently claimed to have found a weak correlation between the X-ray and radio emission of the Seyfert 1 galaxy NGC 4051, but, with Jones et al. (2011) claiming the opposite, the matter is still under debate.

1.1 X-ray Spectral Variability

Variability in the absorption of X-Ray emission from the nuclei of Seyfert 2 Galaxies has been found to be extremely common (Risaliti et al. 2002). By studying the X-ray spectral variability of AGN, it is possible to make constraints on the nature of the environment surrounding the nucleus, thereby also probing the nature of the central object itself. Variability has largely been attributed to changes in the absorbing column between the X-ray source and the observer (Risaliti et al. 2002). The detection of N_H variability on timescales of hours in some Seyfert galaxies has indicated that this absorbing material must be close to the nucleus, at a distance similar to that of the Broad Emission Line Region (e.g. Elvis et al. (2004), Puccetti et al. (2007)). Specific 'occultations', seen as short-term changes in X-ray flux and spectral hardness, have led to claims of direct observations of Broad Line Region Clouds crossing the X-ray source (Risaliti 2007A).

1.2 Cross-Correlation of Multi-Wavelength Observations

Cross-correlation is a method for discovering whether two sets of data are correlated with one another with a given time delay. The method involves 'sliding' one data set across the other and finding the degree of correlation at a range of 'time lags'. Plotting the cross-correlation function (CCF) against the lag will then reveal a lag, if present, as a peak at the lag time by which one data set lags the other.

If lightcurves from two different wavelengths are cross-correlated, any correlation between them will reveal a causal connection between the two sets of emission. In this case, the method is useful for discovering whether variability in radio emission is correlated with that of X-ray emission, as this would require the two to be as a result of the same process. Furthermore, the peak in the correlation coefficient shows the magnitude and 'sign' of any delay between the two data sets, i.e. which data set lags the other and by how long in time.

1.3 Objects

1.3.1 NGC 1365

NGC 1365 is a nearby Seyfert galaxy, observations of which have found it to possess huge spectral variability (Risaliti et al. 2009), on timescales of hours to years, thought to be due to variations in a partially ionised absorber near the X-ray source (Brenneman et al. 2013). Despite the number of studies of this object, all previous work has concentrated on detailed spectral analysis of the system at a single epoch, or short term variability between small numbers of observations. By contrast, in this work we study 50 *SWIFT* spectra taken over a period of six years. This data covers both a significantly longer time period and a far greater flux range than previous studies, allowing the study of long term-trends.

1.3.2 NGC 5548

NGC 5548 is a Seyfert galaxy possessing relatively strong radio emission from its nucleus, in addition to two diffuse, low luminosity lobes (Wilson & Ulvestad 1982). The nucleus was found to be variable in radio by Wroble (2000), indicating that jets are present. Beyond this, little radio data has been published regarding NGC 5548. In this work, we carry out cross-correlation of this system, using simultaneous radio data from the *AMI* radio array and X-ray data from *SWIFT* and the *RXTE*. This has enabled a possible link between X-ray and radio variability to be detected.

2 Current Work

2.1 X-ray Spectral Variability

2.1.1 Observations & Data Reduction

The observations of NGC 1365 were performed using the *SWIFT XRT*, between 21 July 2006 and 17 March 2013. A total of 81 spectra were taken over more than 220 kiloseconds of exposure time. Individual exposure times ranged from < 100 seconds to > 17 kiloseconds. 31 spectra were rejected on the basis of low total counts in the exposure or artifacts near the source, leaving 50 usable spectra, consisting of ~ 140 kiloseconds of data.

The *XRT* data were automatically reduced using version 0.12.4 of the *Swift* XRTPIPELINE software. The XSELECT tool was used to extract background-subtracted spectra and lightcurves. The observed XRT count rates were carefully corrected for the fraction of counts lost due to bad pixels and columns, vignetting effects, and the finite extraction aperture. Fig. 1 shows a lightcurve of the data.

2.1.2 Data Analysis

2.1.2.1 Spectral Hardness

Plots of the hardness ratio against the hard count rate, and the hard count rate against the soft rate of the spectrum are shown in Fig. 2. In each case, hard emission is defined as $2.0-10.0$ keV and soft emission as $0.5-2.0$ keV. The hardness ratio is defined as:

$$\text{Hardness Ratio} = \frac{\text{Hard Counts} - \text{Soft Counts}}{\text{Hard Counts} + \text{Soft Counts}}$$

The plots show the spectrum to be extremely soft at very low fluxes, but to become hard very rapidly with with increasing flux. Beyond this sharp rise, still at relatively low flux, the hardness decreases again more gradually with increasing flux, as often seen in Seyfert galaxies (e.g. Sobolewska & Papadakis (2009), Lamer et al. (2003)). The data display a relatively small amount of scatter about this general trend; for this reason, the shape of the spectrum can be assumed to be approximately similar at a given flux level, independent of time. This implies that the system is behaving in approximately the same manner at each flux level, irrespective of what state the system was in at an earlier time.

2.1.2.2 Spectral Modelling

This similarity in spectral shape allowed spectra of a similar flux to be combined, producing average spectra possessing the average spectral shape at each flux level. This allowed better spectral fits than possible with

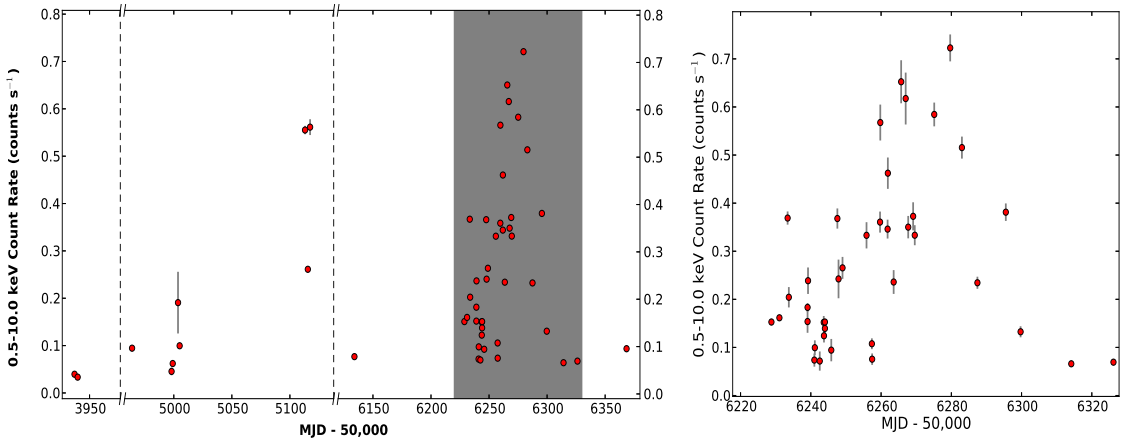

Figure 1. *left:* The SWIFT X-ray lightcurve of NGC 1365, with a broken axis where data was not taken. *right:* The highlighted section of the light curve, during which more intensive *SWIFT* monitoring was taking place, expanded.

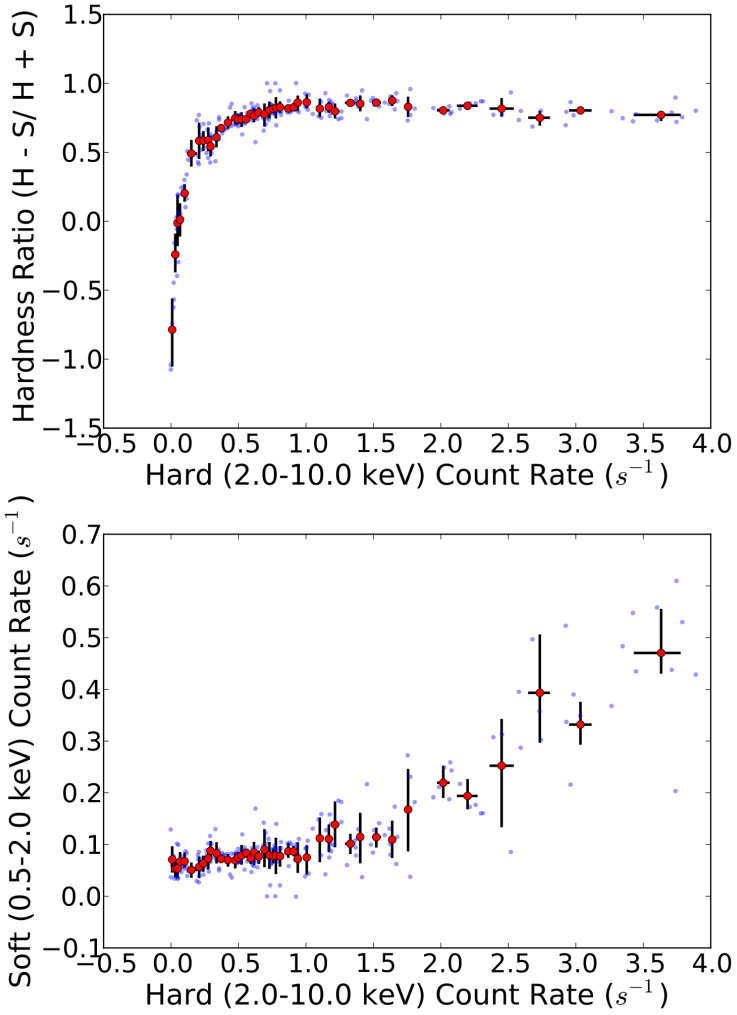

Figure 2. Top: hard count rate against hardness ratio of NGC 1365. Bottom: hard count rate against soft count rate. In each case, the data is binned such that each bin contains a minimum of 5 data points. Errors correspond to one standard deviation of the distribution in each bin.

Model	Parameters			χ^2_{Red}	DoF
	Spectral index	Absorbing column	Ionisation		
Absorbed and unabsorbed power laws	Fixed	Free	Free	1.41	1069
Absorbed and unabsorbed power laws	Fixed	Free	Tied	1.41	1078
Absorbed and unabsorbed power laws	Fixed	Tied	Free	2.42	1078
Absorbed and unabsorbed power laws	Tied	Free	Free	1.17	1068
Absorbed and unabsorbed power laws	Free	Free	Free	1.10	1060
Absorbed and unabsorbed power laws	Free	Free	Tied	1.12	1069
Absorbed and unabsorbed power laws	Free	Tied	Free	1.64	1069
Single, absorbed power law	Free	Free	Free	1.26	1069
Single, absorbed power law	Free	Free	Tied	1.75	1078
Single, absorbed power law	Free	Tied	Free	1.76	1078

Table 1. Summary of the main components of each model fitted to the average spectra, showing the parameters which were fixed, tied or left free in each case, and the reduced χ^2 value and number of degrees of freedom (DoF) of the best fit with each model. Fixed parameters were not allowed to vary. Tied parameters were required to be the same for each of the ten spectra, but allowed to vary. Free parameters were allowed to vary between the fits to individual spectra.

individual spectra. The 50 spectra were divided into 10 flux bins and combined using the *HEADAS* tool 'addspec'. Each of these spectra were then grouped using the *HEADAS* tool 'grpspec' (see Fig. 3).

A variety of models were fitted to the spectra using *XSPEC* (Arnaud 1996). The models were fitted simultaneously to all 10 average spectra, in order discover the cause of variations in the shape of the spectrum with changing flux. It was discovered that a single, absorbed power law of fixed spectral index, fitted the lowest and highest flux observations well, but was insufficient to give a good fit at intermediate fluxes.

Good fits were obtained at all fluxes using a pivoting, absorbed power law, but they required a large range of spectral indices and very low indices at high fluxes, regarded as unlikely in Comptonisation models (Ponti et al. 2006). In previous work, Seyfert galaxies requiring this range of spectral indices have instead been fitted with two-component models with a constant spectral index (e.g. NGC 4051 (Ponti et al. 2006)). Similar two-component models were therefore fitted to the data, consisting of two power laws, one of which is absorbed by material whose absorbing column and/or ionisation state is allowed to vary. This allowed the spectra at all flux levels to be well fit.

The main components of each model are described in Table 1. In models in which the spectral index was fixed, it was set at 1.95, the value found by Risaliti et al. (2013). The absorbed power law used the 'Absori' model for an ionised photoelectric absorber. An emission line, most likely to be due to an iron L-shell transition, was added to all of the models.

Leaving the ionisation state to vary, but tying the absorbing column, was found to be insufficient to account for the degree of variation observed in the spectra, for both a pivoting power law and the two-component model. Tying the ionisation state whilst leaving the absorbing column free to vary, however, gave good fits with the two-component model. Significantly, in the two-component model the χ^2 value remained the same when the ionisation state was tied, as it varied very little even when left free together with the absorbing column. The pivoting, single power law model gives a significantly worse fit in this case. We therefore believe that the two-component model with a varying absorbing column describes the data best.

2.1.2.3 Two-Component Spectral Variability

Fig. 3 shows a sample of the average spectra at different flux levels, fitted with the two-component model described above. In this case, the spectrum is composed of two power laws - an unabsorbed component and an absorbed component, which can be seen to vary by a large degree as the absorbing column changes.

2.1.3 Discussion

2.1.3.1 A Possible Link Between Source Flux and Column Density

An important implication of the best fitting parameters of this model is that the absorbing column of absorbing material seems to be inversely correlated with the normalisation parameter of the absorbed power law, equivalent to the flux prior to absorption (see Fig. 4). As spectral fits show that ionisation changes cannot explain variability, another physical explanation is needed - a possible solution is variations in an 'X-ray wind' of absorbing material rising from the accretion disc.

Fig. 4 also shows the relative variation of the two power law normalisation parameters, demonstrating them to be approximately correlated. This correlation implies that the two components are causally linked, as would be expected if the absorbed component corresponded to direct emission absorbed by material along the line of sight and the unabsorbed component corresponded either to direct emission which has not encountered any absorbing material, i.e. due to partial covering, and/or scattered emission.

2.1.3.2 AGN Wind Model

In the AGN wind model proposed by Elvis (2000), absorbing material arises from a narrow range of accretion disc radii in a biconical 'wind'; in this model an increase in X-ray luminosity causes the opening angle between the wind and the disc to decrease, hypothesised as due to the increased radiation pressure. Models by Nicastro (2000) show that a higher accretion rate could also lead to an increase in the launch radius of the wind. Tombesi et al. (2013) suggested that the X-ray absorbing component of the wind has a density gradient, such that the density decreases with decreasing radius. In the context of the wind model described above, this would mean that a change in the X-ray luminosity of the nucleus would cause a change in the absorbing column through which the source is observed for some viewing angles. If the observer is viewing the X-ray source through an inner part of the X-ray-absorbing wind, an increase in X-ray luminosity would lead to a decrease in the absorbing column of the section of the wind through which the source is being observed. This would lead to a negative correlation

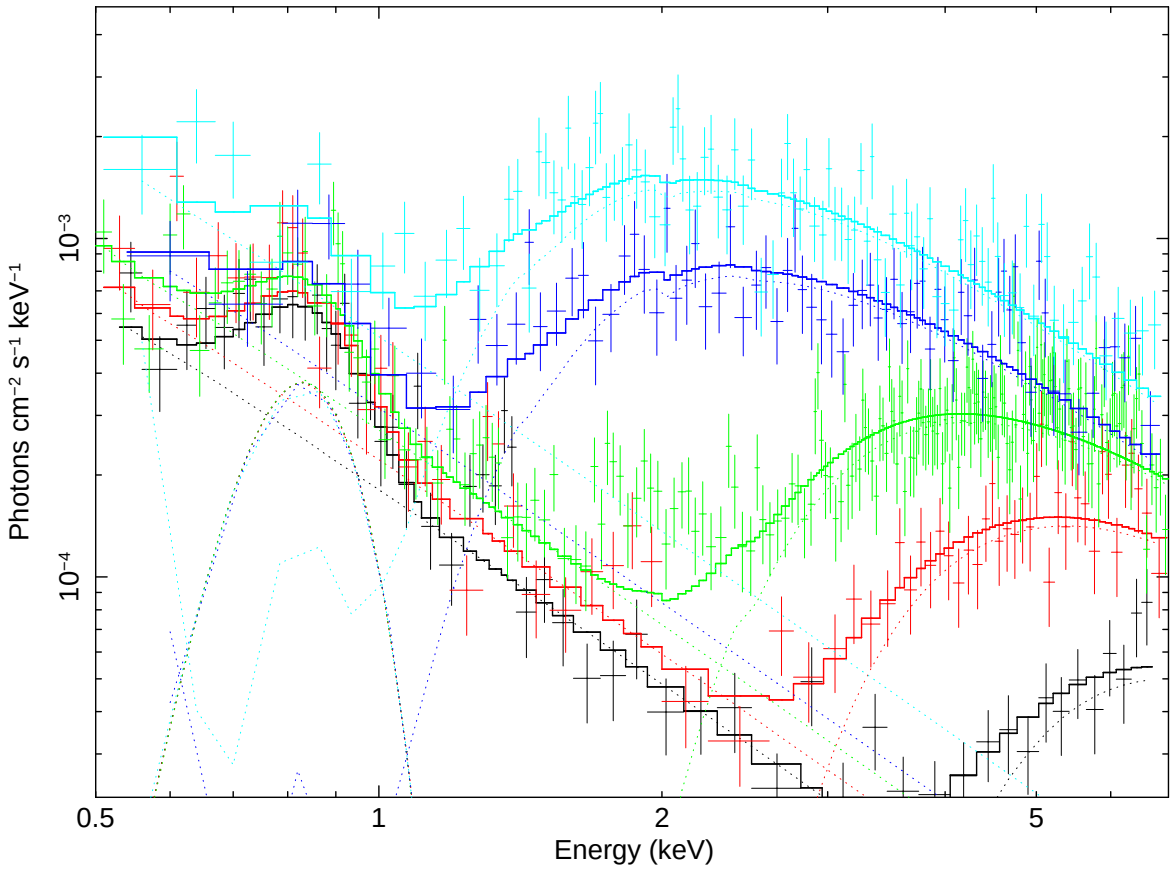

Figure 3. A sample of the set of average spectra produced by combining spectra in the same flux range. The spectra are fitted with the best fitting model, consisting of two power laws, one of which is absorbed and one of which is not.

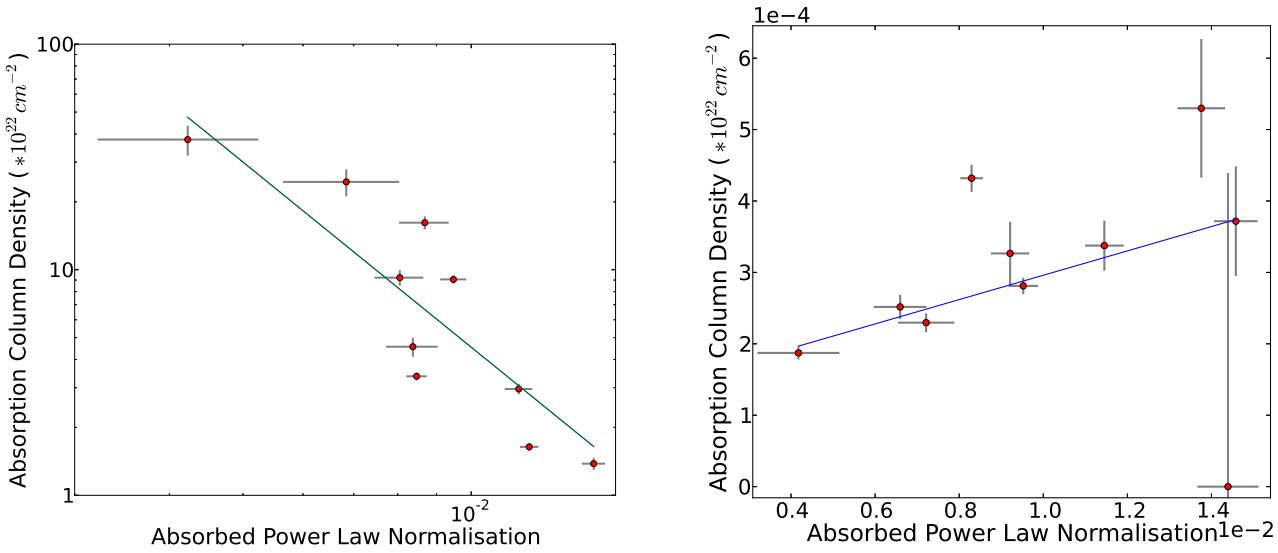

Figure 4. The normalisation parameter of the absorbed power law against the absorbing column of the absorbing material in the model described above.

between the absorbing column of absorbing material and the X-ray luminosity of the nucleus, as found in our spectral fits. The reflected component seen in our spectra could, in this case, correspond to a component of the X-ray emission scattered from the inner edge of the disc wind.

2.2 Cross-Correlation of Multiwavelength Data

2.2.1 Observations & Data Reduction

Data from *SWIFT*, *RXTE* and the *AMI* radio array were all used for this study. The *SWIFT* data was reduced in the same manner as described in section 2.1.1. The *RXTE* and *AMI* data were both reduced, carefully, by others. The combined X-ray lighturve is shown plotted together with the *AMI* radio lightcurve in Fig. 7.

2.2.2 Data analysis

2.2.2.1 Discrete Cross-Correlation

The data were cross-correlated using the 'discrete' method; each mean-subtracted data point in the X-ray data is multiplied by every data point in the the radio data. These values are divided by the product of the standard deviations of both data sets and the total number of data points (N), giving the correlation coefficients:

$$Correlation\ Coefficient = \frac{1}{N}\frac{(x_{t_i} - \bar{x})(y_{t_i} - \bar{y})}{\sigma_x \sigma_y} \tag{1}$$

The time difference between each pair of data points is also found. This gives the correlation coefficient for a large number of exact time lags, but only for single pairs of data points. By binning these data into time lag bins, the average degree of correlation within each time bin can be found, creating a CCF.

2.2.2.2 Lightcurve simulation

It is necessary to create confidence curves in order to be able to determine the significance of any peaks in the CCF. This is achieved by the creation of artificial lightcurves which possess the same statistical properties as one data set, then cross-corellating these lightcurves with the second data set. In this way, the likelihood that peaks in the CCF can be produced randomly can be determined and displayed as confidence curves.

Artificial lightcurves were produced with the Timmer & König (1995) method, using the power spectrum of the real lightcurve. In this case the power spectrum was already known, so values from Uttley (2000) were used - the power spectrum approximately follows a broken power law given by:

$$PSD(\nu) = \begin{cases} \nu^{-\alpha_{low}} & \text{if } \nu <= \nu_{break} \\ \nu_{break}^{\alpha_{high}-\alpha_{low}} \times \nu^{-\alpha_{high}} & \text{if } \nu > \nu_{break} \end{cases} \tag{2}$$

where $PSD(\nu)$ is the power spectral density at frequency ν, the spectral index above and below the break are $\alpha_{low} = 2.40$ and $\alpha_{high} = 1.00$, and $\nu_{break} = 5.14 \times 10^{-5}$ is the break frequency.

For each artificial spectrum created, Gaussian-distributed random numbers are used to produce a 'noisy' periodogram from the power spectrum. The inverse Fourier transform of this is an artificial lightcurve. The mean and standard deviation are adjusted to match those of the original lightcurve, then it is artificially sampled with the same sampling pattern as the data. The result is a lightcurve whose statistical properties are identical to that of the real lightcurve. An example of an artificial lightcurve compared to the real X-ray light curve is shown in Fig. 6.

2.2.2.3 Confidence curves

Confidence curves are created by producing a grid of CCFs for multiple artificial spectra. To find the 90% confidence levels, for example, the 90th quantiles of each time bin divided by the typical peak width in the CCF, calculated by finding the FWHM of the autocorrelation function of the data. These values are then plotted together with the CCF; any peaks which lie above this line can be assumed to be real with a likelihood given by that limit.

2.2.2.4 Results

The CCF for the X-ray and radio data from NGC 5548 is shown in Fig. 5. Two peaks are seen in the data which lie above the 90% confidence level, one at ~ 40 days and one at ~ 120 days. Only the 40 day peak lies above the 99% confidence level, however, meaning this is the the only lag which is very likely to be real.

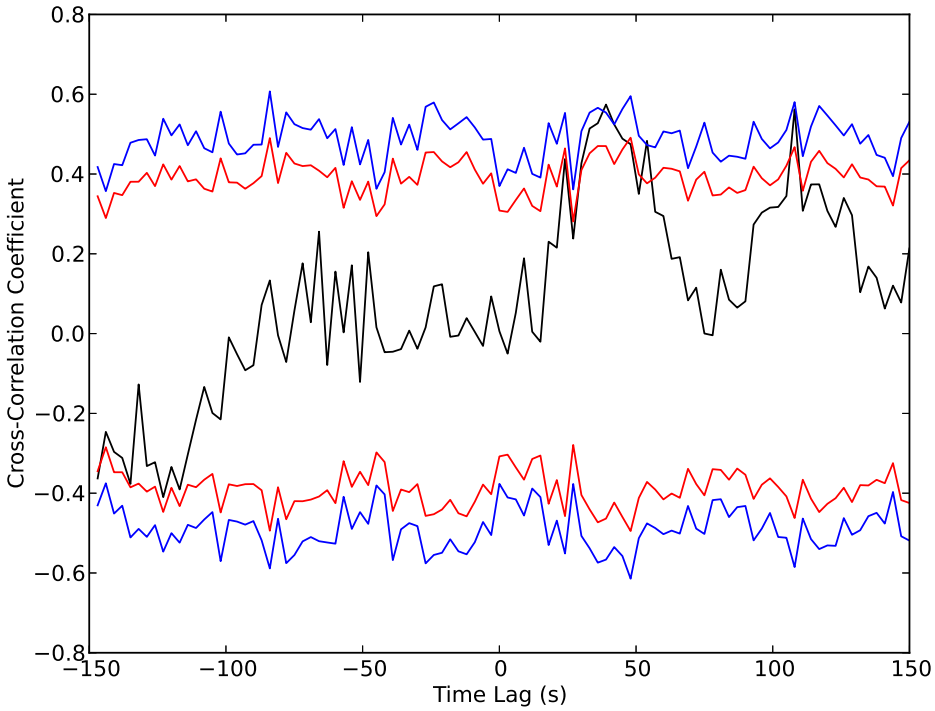

Figure 5. The CCF of NGC 5548; overplotted are the 90% (red) and 99% (blue) confidence levels. The only peak lying above the 99% confidence level hints at a correlation with a delay of ~ 40 days.

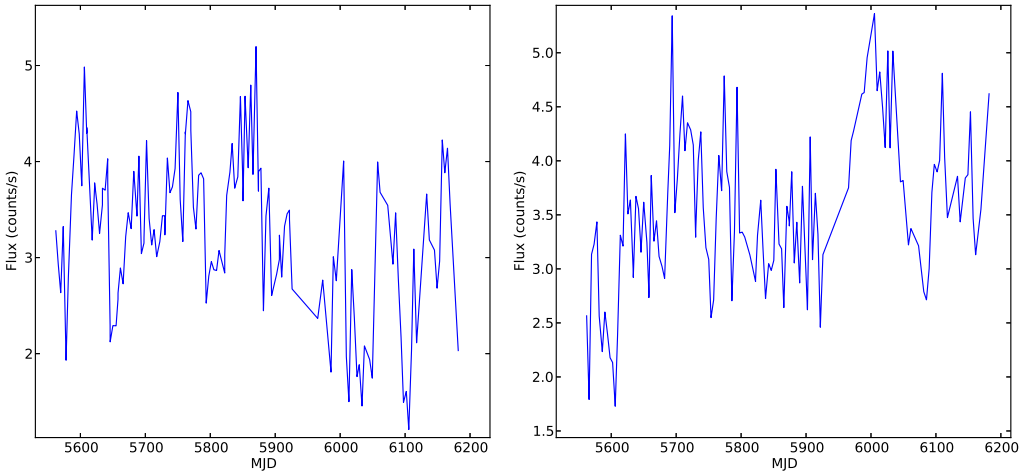

Figure 6. An example of a simulated lightcurve (*right*) compared to the real X-ray lightcurve of NGC 5548 (*left*). The similarity in the variability is readily apparent.

2.2.3 Discussion

The data shows that that the variability in the radio emission lags the variability in the X-ray emission from NGC 5548, by a period of approximately 40 days, with 99% certainty (see Fig. 8). This implies that the same process leads to variability in both sets of emission, indicating the presence of jets. This is incompatible with most definitions of the 'high-soft' state, though a second, similar state for GBHs has been suggested by Gallo et al. (2012) which would be analogous to radio-loud, soft AGN.

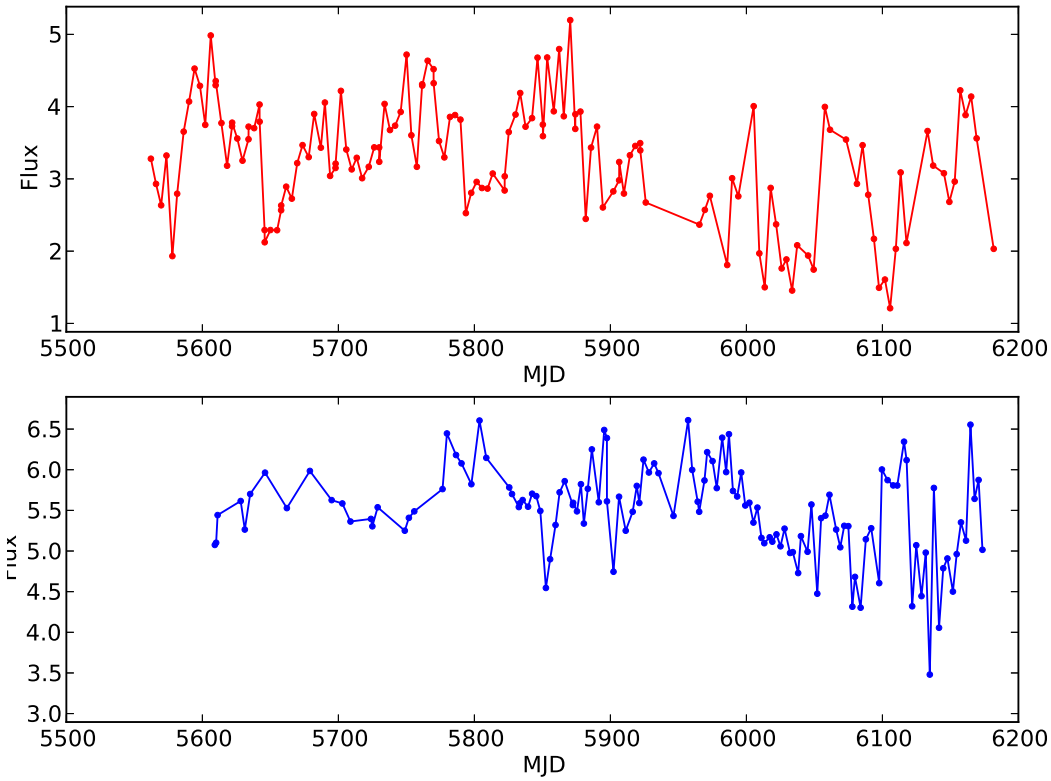

Figure 7. The X-ray (*top*) and radio (*bottom*) lightcurves of NGC 5548.

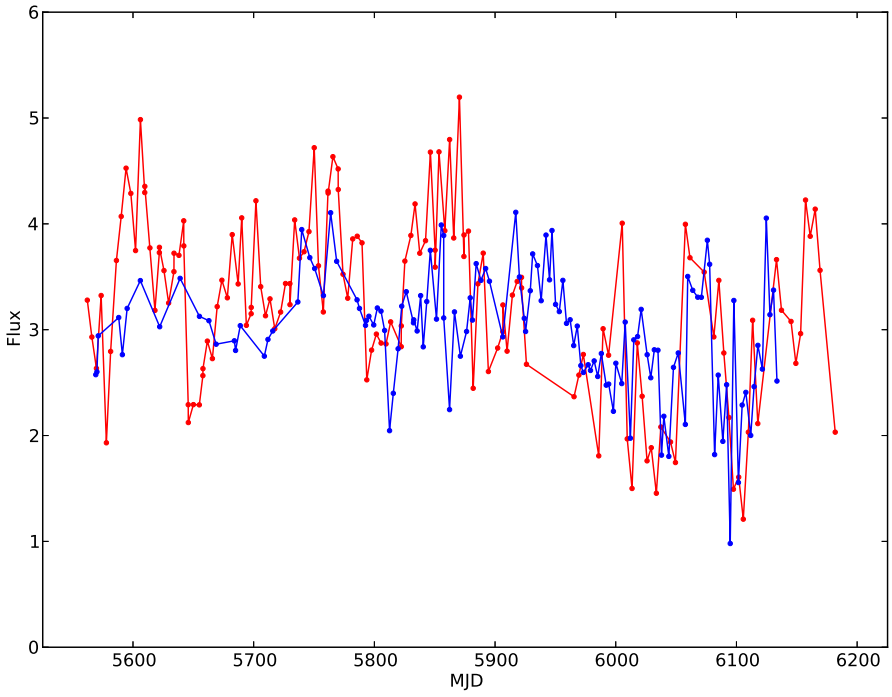

Figure 8. The X-ray (*red*) and radio (*blue*) lightcurves of NGC 5548 overlaid, with a 40 day lag subtracted from the radio data. A similarity in the variation in the lightcurves can be seen by eye.

3 Future Work

3.1 X-ray Spectral Variability

In addition to NGC 1365, a large amount of *SWIFT* data is available on NGC 4395; 225 observations consisting of over 300 kiloseconds, covering a period of over 12 years. NGC 4395 is a Seyfert 1 galaxy possessing huge variability, similar to NGC 1365 (Vaughan et al. 2005). This variability is also seen to be very rapid and has been hypothesised to be at least partly due to variations in an absorber analogous to that proposed here for NGC 1365 (Iwasawa et al. 2000). It is therefore my intention to apply the same methods as used for NGC 1365 to NGC 4395, in order to discover whether there are any parallels between what appear to be similar systems.

3.2 Cross Correlation of Multiwavelength Data

A huge amount of *SWIFT* data is also available on the active nucleus of M81, including data which is simultaneous with data from the *Very Long Baseline Interferometer* (*VLBI*). It is therefore possible to carry out a similar multi-wavelength correlation study on the X-ray and radio emission from this AGN, in order to determine whether any links between these wavebands exist. It is my intention do carry out such a study.

REFERENCES

Arnaud, K.A., 1996, Astronomical Data Analysis Software and Systems V, 101, 17.
Belloni, T. M., 2010, LNP, 794, 53.
Bianchi, S., Maiolino, R., Risaliti, G., 2012, AdAst, 2012, 17.
Brenneman, L. W., Risaliti, G., Elvis, M., Nardini, E., 2013 MNRAS, 429, 2662.
Braito, V., Ballo, L., Reeves, J. N., Risaliti, G., Ptak, A., Turner, T. J., 2012, MNRAS, 428, 2516.
Done, C., Madejski, G. M., Smith, D. A., 1996, ApJ, 463, 63.
Elvis, M., 2000, ApJ, 545, 63.
Elvis, M., Risaliti, G., Nicastro, F., Miller, J. M., Fiore, F., Puccetti, S., 2004, ApJ, 615, 25.
Fabian, A. C., Vaughan, S., 2003, MNRAS, 340, 28.
Fabian, A. C., Zoghbi, A., Ross, R. R., Uttley, P., Gallo, L. C., Brandt, W. N., Blustin, A. J., Boller, T., Caballero-Garcia, M. D., Larsson, J., Miller, J. M., Miniutti, G., Ponti, G., Reis, R. C., Reynolds, C. S., Tanaka, Y., Young, A. J., 2009, Nature, 459, 540.
Fender, R. P., Belloni, T. M., Gallo, E., 2004, MNRAS, 355, 1105.
Fender, R. P., Homan, J., Belloni, T. M., 2009, MNRAS, 396, 1370.
Gallo, E., Miller, B. P., Fender, R., 2012, MNRAS, 423, 590.
Iyomoyo, N., Makishima, K, Fukazawa, Y., Tashiro, M. Ishisaki, Y., 1997, PASJ, 49, 425.
Iwasawa, K., Fabian, A. C., Almaini, O., Lira, P., Lawrence, A., Hayashida, K., Inoue, H., 2000, MNRAS, 318, 879.
Jones, S., McHardy, I., Moss, D., Seymour, N., Breedt, E., Uttley, P., Körding, E., Tudose, V., 2011, MNRAS, 412, 264.
King, A. L., Miller, J. M., Reynolds, M. T., Gultekin, K., Gallo, E., Maitra, D., 2013, arXiv, 1307.5249.
Krolik, J. H., Begelman, M. C., 1988, ApJ, 329, 702.
Krolik, J. H., 1999, 'Active Galactic Nuclei: From the Central Black Hole to the Galactic Environment', Chichester: Princeton University Press.
Lamer, G., McHardy, I. M., Uttley, P., Jahoda, K., 2003, MNRAS, 338, 323.
Lavaux, G., Hudson, M. J., 2011, MNRAS, 416, 2840.
Matt, G., Guainazzi, M., Maiolino, R., 2003, MNRAS, 342, 422.
Markowitz, A., Reeves, J. N., Miniutti, G., Serlemitsos, P., Kunieda, H., Yaqoob, T., Fabian, A. C., Fukazawa, Y., Mushotzky, R., Okajima, T., Gallo, L. C., Awaki, H., Griffiths, R. E., 2008, PASJ, 60, 277.
McHardy, I. M., Papadakis, I. E., Uttley, P., Page, M. J., Mason, K. O., 2004, MNRAS, 348, 783.
McHardy, I. M., Koerding, E., Knigge, C., Uttley, P., Fender, R. P., 2006, Nature, 444, 730.
McClintock, J. E., Remillard, R. A., 2006, 'Black hole binaries', pp 157213.
Mundell C. G., Ferruit P., Nagar N., Wilson A. S., 2009, ApJ, 703, 802.

Neff S. G., de Bruyn A. G., 1983, A&A, 128, 318.
Nicastro, F., 2000, ApJ, 530, 65.
Papadakis, I. E., Sobolewska, M., Arevalo, P., Markowitz, A., McHardy, I. M., Miller, L., Reeves, J. N., Turner, T.J., 2009, A&A, 494, 905.
Ponti, G., Miniutti, G., Cappi, M., Maraschi, L., Fabian, A. C., Iwasawa, K., 2006, MNRAS, 368, 903.
Puccetti, S., Fiore, F., Risaliti, G., Capalbi, M., Elvis, M., Nicastro, F., 2007, MNRAS, 377, 607.
Risaliti, G., Miniutti, G., Evlis, M., Fabbiano, G., Salvati, M., Baldi, A., Braito, V., Bianchi, S., Matt, G., Reeves, J., Soria, R., Zezas, A., 2009, ApJ,696,160.
Risaliti, G., Harrison, F. A., Madsen, K. K., Walton, D. J., Boggs, S. E., Christensen, F. E., Craig, W.W., Grefenstette, B. W., Hailey, C. J., Nardini, E., Stern, D., Zhang, W. W., 2013, Nature, 494, 449.
Risaliti, G., 2007,ASPC, 373, 458
Risaliti, G., Elvis, M., Fabbiano, Baldi, A.,Zezas, A., Salvati, M., 2007, ApJ, 659, 111.
Risaliti, G., Elvis, M., Nicastro, F., 2002, ApJ, 571, 234.
Risaliti, G., Maiolino, R., Bassani, L., A&A, 365, 33.
Risaliti, G.,Bianchi, S., Matt, G., Baldi, A., Elvis, M., Fabbiano, G., Zezas, A., 2005, ApJ, 630, 129.
Risaliti, G., Elvis, M., Fabbiano, G., Baldi, A., Zezas, A., 2005, ApJ, 623, 93.
Sobolewska, M. A., Papadakis, I. E., 2009, MNRAS, 399, 1597.
Stirling, A. M., Spencer, R. E., de la Force, C. J., Garrett, M. A., Fender, R. P., Ogley, R. N., 2001, MNRAS, 327, 1273.
Timmer, J., König, M., 1995, A&A, 300, 707.
Tombesi, F., Cappi, M., Reeves, J., Nemmen, R. S., Braito, V., Gaspari, M., Reynolds, C. S., 2013, MNRAS, 430, 1102.
Urry, C. M., Padovani, P., 1995, PASP, 107, 803.
Uttley, P., 2000, 'Timing Studies of Seyfert Galaxies with the Rossi X-ray Timing Explorer', Ph.D. Thesis, University of Southampton.
Vaughan, S., Iwasawa, K., Fabian, A. C., Hayashida, K., 2005, MNRAS, 356, 524.
Wilson, A. S., Ulvestad, J. S., 1982, ApJ, 260, 56.
Wroble, J. M., 2000, ApJ, 531, 716.